JOURNAL OF GEOPHYSICAL RESEARCH: OCEANS, VOL. 118, 1–15, doi:10.1002/jgrc.20089, 2013

Long-term characteristics of simulated ice deformation in the Baltic Sea (1962–2007)

U. Löptien,[1,2] S. Mårtensson,[1] H.E.M. Meier,[1] and A. Höglund[1]

Received 3 August 2012; revised 19 December 2012; accepted 17 January 2013.

[1] The North Atlantic Oscillation (NAO) index is a frequently used measure for the mean winter conditions in Northern Europe. A positive, high index is associated with strong westerlies and anomalous warm temperatures. The effects on sea ice conditions in the Baltic Sea are twofold. Warm temperatures prevent sea ice formation. If ice is present nevertheless, the strong winds can promote the formation of ice ridges which hinders ship traffic. We use an ocean-sea ice model to investigate the NAO impact on the ridged ice area fraction in the Baltic during 1962–2007. Our simulations indicate that in the northern Bothnian Bay, a high NAO index is related to an anomalous accumulation of ridges, while in the rest of the Baltic Sea, the relationship is contrary. The NAO explains locally at most only 20–25% of the ridged ice fraction interannual variability which indicates the systems complexity. However, we find high skill with local correlations around 0.8 for annually averaged ridged ice fraction reconstructed from multilinear regression using winter averaged wind extremes, surface air temperature, and sea surface temperature (SST). This suggests that the amount of ridged ice in late winter can be derived from these routinely measured quantities. In large parts of the basin, it is sufficient to use the atmospheric parameters as a predictor, while in the eastern Bothnian Bay and southern Gulf of Finland, the SST is required to reconstruct the bulk of the ridged ice fraction.

Citation: Löptien, U., S. Mårtensson, H. E. M. Meier, and A. Höglund (2013), Long-term characteristics of simulated ice deformation in the Baltic Sea (1962–2007), *J. Geophys. Res. Oceans, 118*, doi:10.1002/jgrc.20089.

1. Introduction

[2] The Baltic Sea is a shallow, brackish sea located in Northern Europe. It is divided into several sub-basins. Three of the major sub-basins are ice covered almost every winter: the Gulf of Finland, the Bothnian Sea, and Bothnian Bay (Figure 1). The climate is dominated by westerlies [*Lehmann et al*., 2011], and accordingly, in all three sub-basins south-westerly winds prevail, having a somewhat more southerly component in the northern Baltic compared to the Gulf of Finland (Figure 2). This wind distribution leads to upwelling in the western part and downwelling in the eastern part of the Baltic Sea basin. Typically, the mean winter conditions are characterized to first order by the North Atlantic Oscillation (NAO) [*Hurrell and Deser*, 2009]. An anomalous high NAO index (>0.5) reflects strong westerlies and consequently rather mild winter conditions in Europe and is related to warmer winters by *2K* in the Baltic Sea region compared to anomalous low index years (<-0.5). At the same time, the strength of the westerlies deviates by a factor of 2 [*Vihma and Haapala*, 2009]. The NAO index is frequently used in climate-related studies [e.g., *Monahan et al*., 2000] and past climate reconstructions [e.g., *Timm et al*., 2004]. In the Baltic Sea region, the NAO is often applied as proxy for the large-scale circulation that controls the local climate and is related to physical, chemical, and biological processes. Its influence on sea ice extent is of general interest, especially for shipping. The ice season lasts up to 7 months, in particular in the northern part of the basin [*Vihma and Haapala*, 2009]. The maximum ice extent is usually reached in late February. On average, the ice covers 45% of the Baltic Sea basin between mid-February and mid-March. Deviations from this mean can be very large, and the maximum ice extent varied between 12.5% and 100% in the last century [*Leppäranta and Myrberg*, 2009]. Close to the coasts, the ice usually appears as fast ice, while the ice is adrift elsewhere. Triggered by frequent storms, convergent ice motion leads to deformations of the ice pack. The most important deformed ice type is ridged ice [*Leppäranta and Hakala*, 1992], which can become 5–15 m thick and accounts for 10–50% of the total sea ice volume in the Baltic [*Leppäranta and Myrberg*, 2009]. Ridges form substantial obstacles to the winter navigation of ships, and the location and severity of ridged ice fields are of general interest [e.g., *Haapala*, 2000; *Kankaanpää*, 1988; *Leppäranta and Hakala*, 1992; *Leppäranta et al*., 1995] This holds in particular since the Baltic is a densely populated area with increasingly high ship traffic. Important shipping

[1]Swedish Meteorological and Hydrological Institute (SMHI), Norrköping, Sweden.
[2]Helmholtz Centre for Ocean Research Kiel (GEOMAR), Kiel, Germany.

Corresponding author: U. Löptien, Swedish Meteorological and Hydrological Institute (SMHI), Folkborgsvägen 1, S - 601 76 Norrköping, Sweden. (ulrike.loptien@smhi.se)

2169-9275/13/10.1002/jgrc.20089

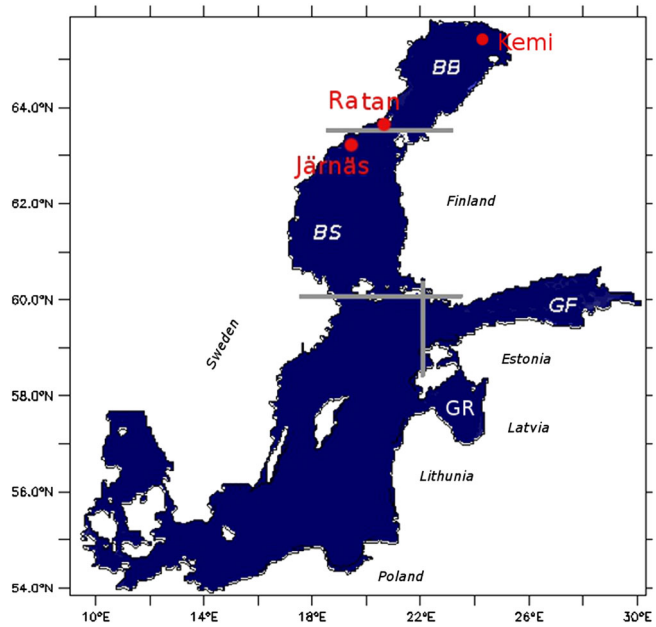

Figure 1. The model domain of the ocean-ice model. Monitoring stations are shown in red, while the white letters refer to the investigated sub-basins (BB = Bothnian Bay, BS = Bothnian Sea, GF = Gulf of Finland, GR = Gulf of Riga). The gray lines depict the basin borders.

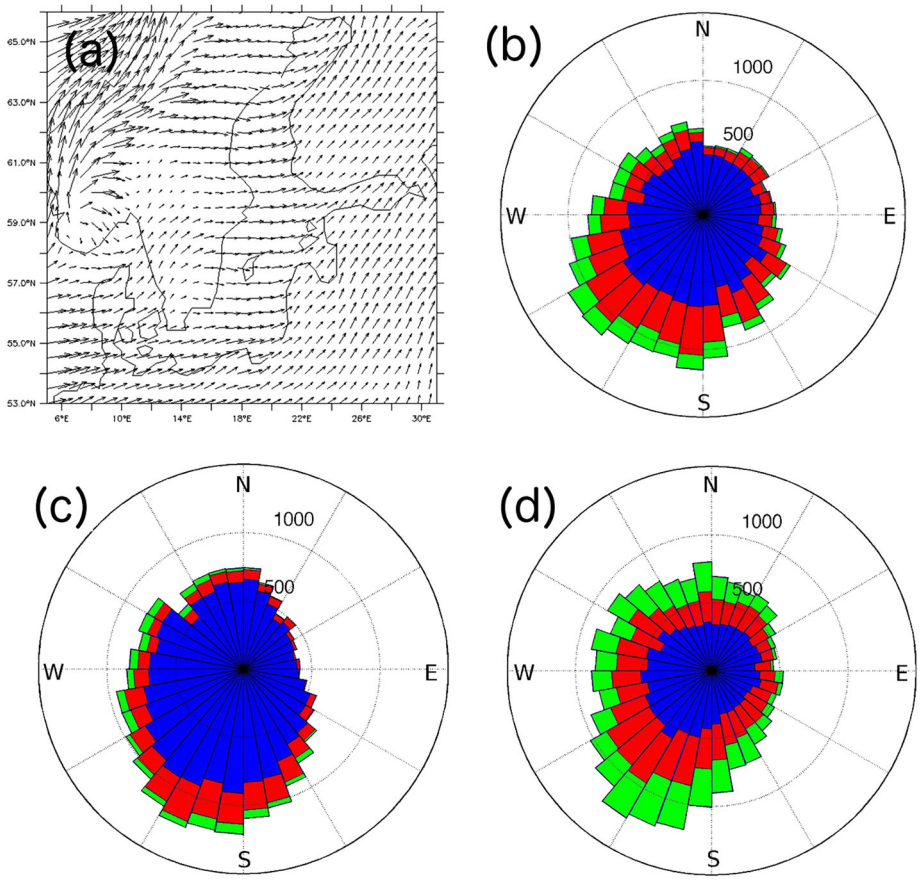

Figure 2. (a) Winter mean wind field based on downscaled ERA-40 data in the Baltic Sea region (1962–2007). Frequency distribution of wind directions in winter over (b) the Gulf of Finland (22°E–30°E, 59°N–61°N), (c) Bothnian Bay (18°E–24°E, 63.5°N–68°N), and (d) Bothnian Sea (16°E–22°E, 60°N–63.5°N). Blue areas correspond to wind speeds of less than 4 Beaufort (Bft), red to wind speed between 4 and 5 Bft and green to 5 Bft and more.

routes cross seasonally ice-covered regions. Hence, sea ice ridges are routinely charted, i.e., real-time information about the Baltic Sea ice conditions are provided by for instance the Swedish (SMHI) and Finnish weather services (FMI). The ice information is based on coastal stations, ship reports, and satellite images. Even so, the specified information about ridges is rather vague, and comprehensive long-term observations of ridges are missing. Accordingly, the evaluation of ice deformation in sea ice models is limited, and an extensive analysis of the statistics of Baltic Sea ice ridges does not yet exist [*Vihma and Haapala*, 2009].

[3] We aim to identify patterns of largest interannual variability and to determine the main drivers and suitable proxies which might help to understand past variability and to assess the risk of ridging in a certain region. As a first step, we focus on the NAO index, whereas the second step aims to build a proxy from winds and air temperature. While wind is a direct driver of ridging, interannual variations in surface air temperature (linked to the NAO) [*Rogers*, 1997] influence the variability of the total sea ice coverage of the Baltic, as shown by earlier studies [e.g., *Tinz*, 1996]. In this respect, it is also a driver of the interannual variability of ridged ice fraction since, e.g., a late onset of the ice growth season increases the probability for less ridges being formed over the rest of the winter, and also the timing of the ice melt in spring affects the ridged ice fraction. Additionally, locally high ice concentrations are a prerequisite for ridging. Thus, a change in ridged ice fraction is indirectly influenced by air temperature.

[4] The determination of suited proxies might in turn help to define time and location for future measurements that can be used for further model improvements. To obtain a reliable statistic, a sufficient long time period with high data coverage is required to separate the major pattern from small-scale noise, such as ridges produced by ships themselves. In the absence of an adequate amount of reliable measurements, we are focusing on modeling results. The analysis is based on a 40 year hindcast simulation of the coupled ocean-ice model RCO (Rossby Centre Regional Ocean model) that was extended by the "Helsinki multicategory ice model" (HELMI) [*Haapala*, 2000; *Haapala et al*., 2005] to resolve undeformed ice in various thicknesses as well as rafted and ridged ice.

[5] The paper is organized as follows. The ocean and ice model as well as observational data sources and statistical methods are described in section 2. This section is followed by a model evaluation part (section 3) and the statistical results (section 4). The paper ends with a discussion part (section 4) and a summary (section 5).

2. Methods

2.1. The Ocean Model

[6] The present study is based on a three-dimensional (3-D) coupled ice-ocean model. The ocean component consists of the Rossby Centre Regional Ocean model RCO. The model is described in more detail in, e.g., *Meier et al.* [2003] and *Meier and Kauker* [2003]. RCO is a regionalized, further development of the Ocean Circulation Climate Advanced Model (OCCAM) [*Webb et al*., 1997] implemented for the Baltic Sea. The model domain covers the Baltic Sea including Kattegat. The model depths are based on a realistic bottom topography taken from *Seifert and Kayser* [1995]. The horizontal resolution is 2 nautical miles. The vertical resolution was recently increased to 83 vertical levels with a constant layer thickness of 3 m. Near-surface temperatures and salinity closely resemble the former 41 level version as presented for instance by *Löptien and Meier* [2011] and *Meier et al.* [1999]. Surface restoring is not applied. As surface boundary conditions (air temperature, wind, cloud cover, sea level pressure, humidity, and precipitation), we use dynamically downscaled ERA-40 reanalysis data [*Uppala et al*., 2006] which were updated with operational European Centre for Medium-Range Weather Forecasts (ECMWF) data. Note that the crossover from ERA-40 to the operational ECMWF data might lead to some discontinuity which might occur in the downscaled data set as well. The same holds for variations in time in the number of operational data included in the ERA-40 data set. The dynamical downscaling is performed by using a regional climate model, the Rossby Centre Regional Atmosphere model version 3 (RCA3) at 25 km horizontal resolution [*Samuelsson et al*., 2011]. Since the surface wind fields were underestimated, a gustiness parametrization is applied. This parametrization is based on an empirical linear relationship between wind gusts and mean wind speed [*Höglund et al*., 2009]. This data set was successfully used as forcing for RCO in many climate-related studies before [e.g., *Meier and Kauker*, 2003; *Meier*, 2006; *Hordoir and Meier*, 2010; *Löptien and Meier*, 2011]. Note, however, that the downscaled forcing provides a very good climatology, but it is not well suited for studying particular, short periods of time. Thus, all comparisons to observations are performed in a statistical sense.

2.2. Sea Ice Model

[7] The original ice model in RCO is a Hibler-type, dynamic-thermodynamic sea ice model with an elastic-viscous-plastic solver for the viscous-plastic rheology [*Hunke and Dukowicz*, 1997] and three-layer thermodynamics [*Semtner*, 1976], based on a single-ice category along with an open-water fraction. A detailed description is given in *Meier et al*. [1999]. We extended this model to resolve different classes of undeformed ice as well as rafted and ridged ice. The latest version is built upon the HELMI [*Haapala*, 2000; *Haapala et al*., 2005; *Mårtensson et al*., 2012], which includes the ice thickness distribution, i.e., ice concentrations of variable thickness categories, and mechanical redistribution of the ice due to deformations and ice strength. Beside the ability to explicitly model deformed ice, HELMI allows, furthermore, for a more detailed description of the ice strength. In the Arctic version, the model improvements were shown to affect the sea ice growth rate and surface albedo [*Mårtensson et al*., 2012; *Holland et al*., 2006] Our model setup deviates slightly from the original HELMI version and is described in detail by *Mårtensson et al*. [2012]. Additional changes include an update to another common calculation of ridged ice thickness ($h_{ri} = 17.64 h_u^{0.5}$ [*Kankaanpää*, 1997], where h_u denoted the undeformed ice thickness (cm)) and an adjusted threshold thickness of 8 cm to Baltic Sea conditions. If the ice is thicker than this threshold, ridging dominates, while rafting dominates for thinner ice [*Parmerter*, 1975]. We adopted all applicable parameter settings from the original ice model in RCO. One exception

is the relatively high harmonic diffusion which reduces the spatial gradient of the modeled ice properties. To lower this effect while still ensuring stability of the model, the diffusion is lowered by a factor of 2, resulting in a value of $2 \cdot 10^2\,m^2/s$. Also, the ice strength is increased by a factor of 5 compared to *Haapala et al*. [2005] since we overestimated the speed of slow-moving ice before which led to an unrealistically high amount of rafted ice compared to ridged ice.

[8] Prognostic variables for ridges are ridged ice thickness and ridged ice concentration. The latter is defined as the areal fraction of a model grid cell covered by ridged ice. In contrast, our best observations of the amount of ridged ice in the Baltic are provided as ridge density (D) defined as number of ridges per kilometer in ice-covered regions. Therefore, a function relating the model variables to this observed quantity is required and has to be parameterized from the mean ridged ice thickness per grid box, which implicitly includes ridged ice concentration. We follow the approach of *Lensu* [2003]:

$$D = 1/0.15 \frac{h_r}{H^2}. \quad (1)$$

[9] Here, h_r denotes the simulated mean ridged ice thickness (m) per grid box and H the mean ridge sail height, which is derived from observations and accordingly set to 1.4 m. The factor 0.15 is chosen to match the available data best out of possible values ranging from 0.123 to 0.317 [*Lensu*, 2003]. The ridge density is considered per ice-covered area. Note that the simulated ridged ice volume does not take porosity into account, while observations suggest an average porosity of approximately 30% [*Lensu*, 2003]. When comparing to observed ridge density as well as helicopter-borne measurements of ice thickness, we increase the ridged ice volume accordingly. All figures that do not refer to a direct comparison with observations show the original model output without accounting for porosity. For the analysis of the deformed ice characteristics, we consider the whole simulation period 1962–2007. The annual mean for the ice variables neglects the predominantly ice-free months and refers to an average of the months December to April (DJFMA). The analyzed atmospheric variables are averaged over the same period and refer thus to winter mean values.

2.3. Data Sources

[10] For the model evaluation, the model results are compared to various observational data sets. Sea ice extent for the period 1980–2007 is derived from the BASIS data set [*Udin et al*., 1981], an ice data base for the Baltic Sea constructed from ice charts provided by the ice services. The data set was developed as a joint project of the former "Finnish Institute for Marine Research" (FIMR) and the "Swedish Meteorological and Hydrological Institute" (SMHI). More detailed information of the climatological ice properties, including level ice thickness (=undeformed ice), ice concentration, and dominant ice type, are taken from the "Climatological Ice Atlas for the Baltic Sea, Kattegat, Skagerrak and Lake Vänern (1963–1979)" by [*SMHI and FIMR*, 1982]. The Ice Atlas contains long-term average observations from SMHI and FIMR. The thermodynamics of the model is tested in more detail by considering weekly ice thickness measurements from drill holes (1971–2007 and 1976–2007) in the fast-ice zone at the stations Järnäs (19.41°E 63.2°N) and Ratan (20.54°E 64.0°N) in the Bothnian Sea (Figure 1). The measurements originate from singular measurements close to the coast. The data were provided by the Swedish ice service of SMHI.

[11] To account as well for the model dynamics, airborne EM-thickness measurements (= electromagnetic sounding) in the sub-basin interiors of the Gulf of Finland and Bothnian Bay are considered. The data were collected from four measurement campaigns during the period 2003–2007 by Christian Haas within the IRIS project [*Haas*, 2004]. The EM method is a relatively newly developed small, digitally operated frequency-domain electromagnetic-induction system, taking advantage of the fact that sea ice has, in contrast to seawater, a very low electrical conductivity. It allows for the determination of the seawater-ice interface and is generally combined with a laser altimeter which measures the height of the EM system above the ice surface. The method and its accuracy are discussed in more detail by *Haas et al*., [2009]. Note that the EM method cannot distinguish between snow and ice and therefore gives total snow and ice thickness. For comparison with the model, all observational data (from the Bothnian Bay, Bothnian Sea, and Gulf of Finland) are combined in one data set. To ensure comparability, the EM data were mapped onto the RCO grid, and for each flight, corresponding ice thicknesses where extracted from the model using snapshots closest in time to each flight. But still, model and observations result from different spatial scales, and it is implicitly assumed that the helicopter track is representative for the whole model grid-box domain which might not be the case. Unfortunately, there is no "perfect" solution to compare data from different spatial scales. The data coverage of the EM data is sufficiently high, and altogether the EM data cover 1010 model grid points, not counting overlapping tracks more than once. Additionally, ice drift data from two buoys in the Bothnian Bay were collected within the same project and were provided by Karin Borenäs (personal communication, 2012). The corresponding measurement campaign lasted from March to May 2004. From these buoy positions, ice velocities were computed as the distance traveled by the buoy between 1 h intervals. Pairs with longer intervals between them were not used. For comparison to the observed buoy velocities, six-hourly snapshots of the simulation matching best in time were considered. Data with buoy positions within the fast ice are neglected. Operational digitized ice charts, called IceMap, from the Swedish Ice Service at SMHI were extended in 2006 to include ridge density. The data originate from ship observations, rating the ice conditions on a discrete scale. As such, they are approximate only but are useful for evaluating the position and the relative characteristics of ridged ice in the Baltic.

2.4. Statistical Methods

[12] Most of the statistical analysis is based on linear correlations (Pearson's product-moment coefficient), which measures the relationship between two data sets. To get closer to normal distribution, ridged and rafted ice fraction are transformed by taking the square root before calculating the correlations. Note that nonlinear relationships will not be fully determined but approximated linearly. For those areas

with rare ice coverage, the correlations are patchy due to missing values. In some instances, correlations are expressed as explained variances (=square of the correlation) which measure the proportion to which a mathematical model accounts for the variation of a given data set, i.e., give the "percentage of variance explained" by the linear regression. The atmospheric data are taken from the forcing data set of the ocean-ice model and averaged from December to April (DJFMA) to match the ice season. To account for expected nonlinearities when investigating the winds, we consider seasonal mean wind speed, mean of the square of the wind speed (which is related to wind stress), and the wind extremes. All variables are considered for the cardinal wind directions (north, south, east, and west) separately. As wind extremes, we choose the most extreme wind events (=maximum wind speed per direction) selected locally from six-hourly snapshots for every month. In a second step, the monthly extremes are averaged over season.

[13] Additionally, linear and multilinear regressions are performed. For the multilinear regression, we use sea surface temperature (SST), air temperature (TMP), and wind extremes in the four cardinal directions (WNDN, WNDS, WNDE, WNDW) as regressors and the square root of ridged ice fraction (RFRAC) as response variable, resulting in the following statistical model:

$$\mathrm{RFRAC}_t = \beta_1 + \beta_2 \cdot SST_t + \beta_3 \cdot TMP_t + \beta_4 \cdot WNDN_t + \beta_5 \cdot WNDS_t + \beta_6 \cdot WNDE_t + \beta_7 \cdot WNDW_t + \varepsilon_t.$$

[14] The subscript "t" stands for time, ε_t represents unobserved random noise (=residuum), and the parameters $\beta_1, \ldots, \beta_7$ are estimated by using an ordinary least square fit. A second linear regression is based on ice concentrations and wind extremes in the four cardinal directions instead.

3. Model Evaluation

[15] Figure 3 shows the interannual variability as well as the mean seasonal cycle for simulated and observed ice extent. The interannual variability is reproduced very well. Also the seasonal cycle shows good agreement with the observations, in particular in terms of onset and end of the ice season. Nevertheless, sea ice extent is on average slightly overestimated by the model, especially in March. Simulated long-term mean level ice thickness and concentration are depicted in Figure 4 for February (1963–1979). February is chosen since it typically reflects the time of maximum ice extent. The corresponding figures from the Climatological Ice Atlas from *SMHI and FIMR* [1982] are depicted below (Figures 4c and 4d). Except in the Gulf of Riga and the interior of the Bothnian Bay, where ice concentrations are too low in the model, ice concentrations are comparable to the Ice Atlas, while the level ice thickness is underestimated. The local maximum level ice thickness occurs in the fast-ice zone in the Bothnian Bay with simulated values in the range of 35–50 cm, while the Ice Atlas shows values of 50–70 cm. In mid-February, ice thickness in the center of the Bothnian Bay ranges between 25 and 30 cm, while it is indicated with 30–50 cm in the Ice Atlas. Also, in the Gulf of Finland the ice thickness is underestimated by 10–15 cm.

[16] To evaluate the thermodynamics of the model in more detail, model data are compared to drill holes in the fast-ice zone. Observed and simulated mean seasonal cycles from stations Järnäs and Ratan are depicted in Figure 5. To match thick coastal fast ice best, the thickest undeformed ice category is compared to the station measurements. This data set confirms that the ice thickness is systematically underestimated by 10–15 cm. In Ratan, the shapes of the mean seasonal cycles are very similar, and the model bias in Ratan appears as an almost constant offset, while the ice model underestimates the thickness only slightly at the start of the season in Järnäs. Here, the bias increases throughout the season. The standard deviations are similar in both model and observations. Note that the drill hole for both stations are located very close to the coast and might thus be not fully representative for the whole model grid box. Also, especially the grid box from station Järnäs contains some unrealistic deformed ice fraction which is due to the relatively high diffusion in the model. *Saloranta* [2000] sampled snow and ice thicknesses at station Kemi (their Figure 4). Our simulated seasonal cycle at this location (Figure 6) agrees generally well with their results, while some minor differences occur. In comparison, the simulated ice is about 10 cm thinner at the maximum, and snow accumulation in January/February is weaker than observed. Although the length of the ice

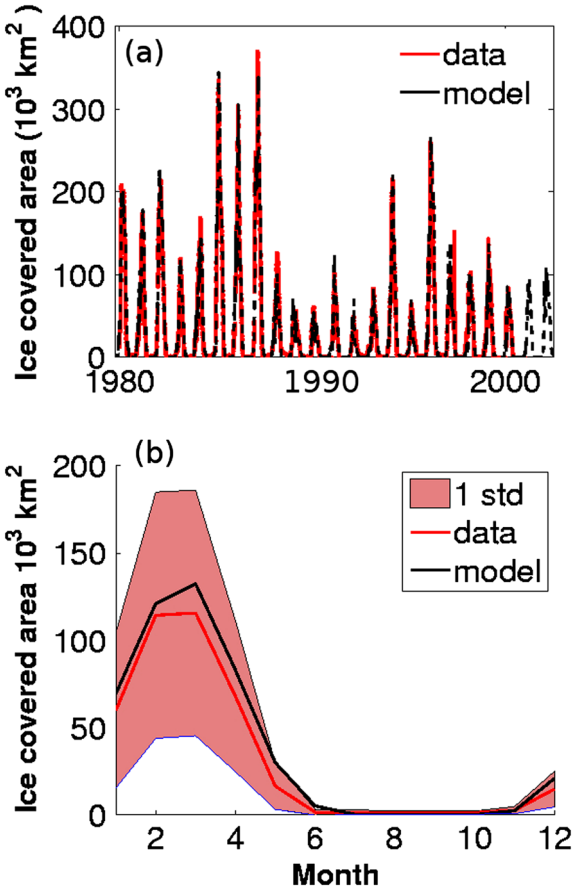

Figure 3. (a) Modeled ice extent (black line) compared to observations [*Udin et al.*, 1981] (red line) and (b) mean seasonal cycle of simulated and observed ice extent. The red shaded area refers to the standard deviation of the observations.

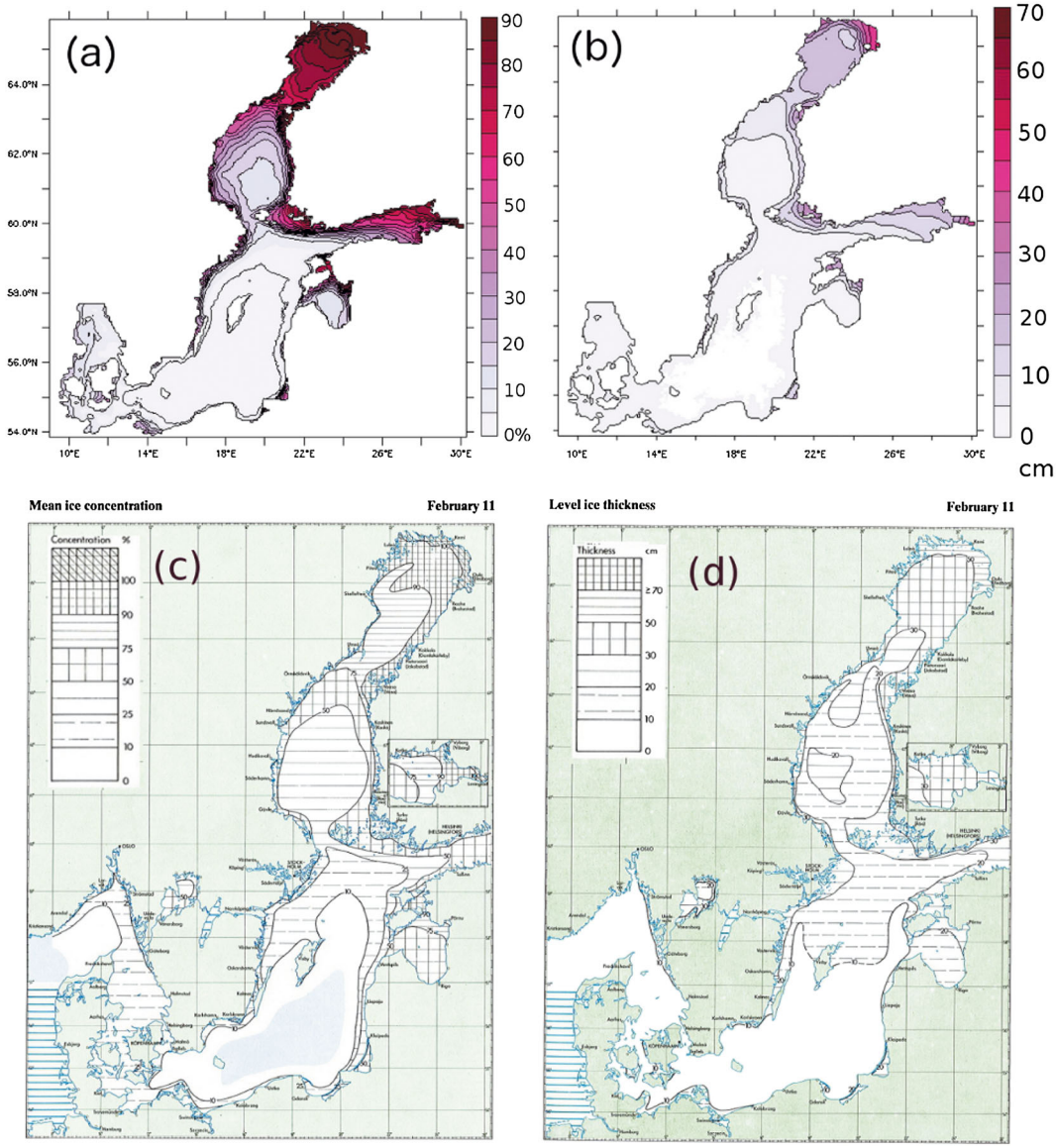

Figure 4. Simulated long-term mean of (a) ice concentrations [%] and (b) level ice thickness [cm] in February. The lowest level corresponds to a thickness of 1 cm. The climatological values refer, in accordance to the observations, to the period 1963–1979. The figures below depict the corresponding figures from the "Climatological Ice Atlas, SMHI and FIMR [1982]" in mid-February.

season and timing of the maximum ice and snow thickness agree well with Saloranta's results.

[17] While the mean ice concentration and thickness in the Baltic Sea are relatively well observed, more comprehensive information, e.g., about ridged ice or ice velocity, are difficult to obtain. Figure 7a depicts a histogram of several airborne EM measurements of ice thickness distributions in the Bothnian Bay, Bothnian Sea, and Gulf of Finland when all observational data were combined in one data set. The corresponding helicopter tracks are depicted in Figure 7b. The histogram for the simulated data (in blue) is overlayed with the observational data (in red). For the modeled ridged ice, we account for porosity for this comparison. Again, it becomes apparent that the model underestimates the thickness compared to the EM measurements. Especially the extremes are not captured. The latter can very likely be attributed to the relatively high diffusion in the model. Otherwise, the shape of both histograms agrees well.

[18] Additionally, ice velocities are considered since realistic ice velocities are a prerequisite to model a good representation of ridges. The velocity data were collected during the period March to May 2004 in the Bothnian Bay. In total, only velocities from 28 model snapshots (six-hourly model output) were suited for comparison to the observations. Unfortunately, the available data coverage is thus too sparse to estimate robust histograms and statistical quantities. The three most extreme observed ice velocities (60 cm/s, 45 cm/s, 24 cm/s) are not captured by the model. Deviations between data and model are skewed positively, i.e., high ice velocities are not captured by the model which might partly refer to the

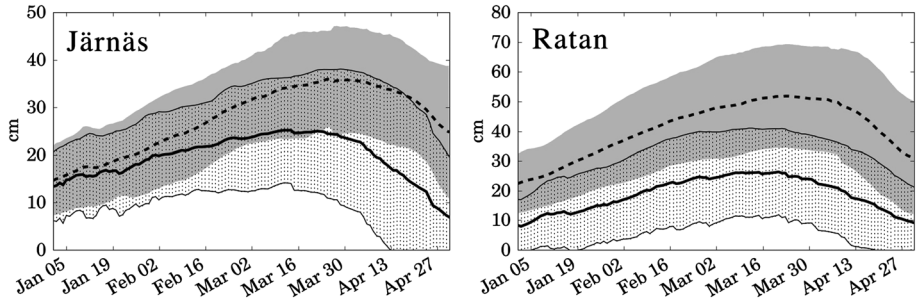

Figure 5. Mean seasonal cycle from January to April for modeled level ice thickness (thick black line) and drill hole observations (dashed black line) at the stations Järnäs and Ratan. The seasonal cycles are derived from the period 1976–2007 for the station Järnäs and 1971–2007 for Ratan. Light gray and gray shading indicates the standard deviations for modeled and observational data, respectively. Observations are provided by the Swedish Ice Service. The left panel corresponds to the station Järnäs and the right panel to the station Ratan (cf. Fig.1).

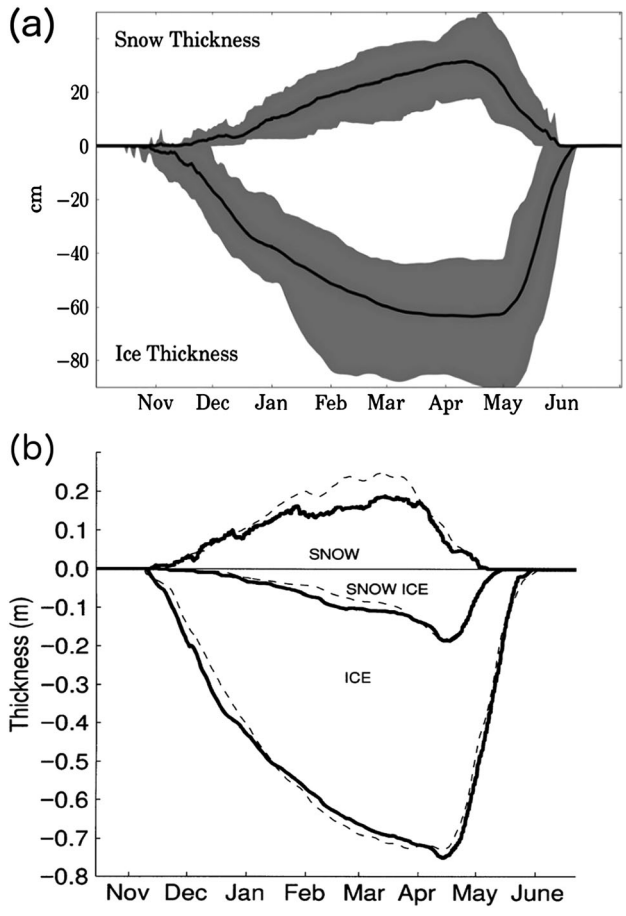

Figure 6. (a) Simulated seasonal cycle of ice and snow thickness at station Kemi (24.31°E 65.4°N) showing the mean (thick black line) and the 5 and 95 percentiles (shaded area) during the period 1979–1990. (b) Modeled mean snow, snow ice, and total ice thickness (solid lines) from the same period by *Saloranta* [2000]. Dashed lines depict the corresponding observed mean thicknesses. The figure is reproduced with permission of Tellus A.

model resolution. Of the differences between observations and model, 75% are in the range of −2 to 10 cm/s, and 40% are in the range of 0 to 3 cm/s.

[19] Although ice charts, provided by the national ice services, contain only rough information about ridges derived from satellite data, a visual inspection of typical regions with deformed ice shows a satisfactory agreement with the model. Since 2006, ice charts (IceMap) from the Swedish Ice Service at SMHI include some estimates of ridge density. Figure 8 depicts the annual mean ridge density during the two winters, 2005–2006 and 2006–2007. Note that ridge density is not a prognostic variable in the model and is diagnosed, as described in section 2. In regions of rare ship traffic, such as most parts of the Bothnian Bay, data coverage is sparse. The fast-ice zone in the Bothnian Bay extends much further in the observations than in the model which results in some differences in the patterns of ridged ice in both data sets. Maximum values agree reasonably well in the Bothnian Bay, while the amount of ridges is underestimated in the Gulf of Finland and, in particular, in the Gulf of Riga. The latter is very likely related to the underestimated ice concentrations in the Gulf of Riga. Due to the relatively high diffusion in the ice model, the gradient from high to low ridge density is comparatively smooth, and small-scale features cannot be reproduced. This includes ridging possibly triggered by intense ship traffic.

4. Results

4.1. Modeled Characteristics of Baltic Sea Ice Ridges

[20] Sea ice ridges form frequently in the northern part of the Baltic Sea (Bothnian Bay and Bothnian Sea) as well as in the Gulf of Finland and Gulf of Riga (Figure 9). Maximum concentrations occur mainly at the northeast side of the sub-basins in agreement with the major wind directions (Figure 2), which indicates a strong wind influence. The mean thickness of ridged ice (Figure 9b) shows a more zonal structure, which is temperature rather than wind related and resembles very much the distribution of level ice thickness. Concentrations as well as thicknesses show large variations on both seasonal and interannual time scales. The pointwise standard deviations of annual mean ridged ice concentration and thickness are depicted in Figures 9c and 9d. The spatial

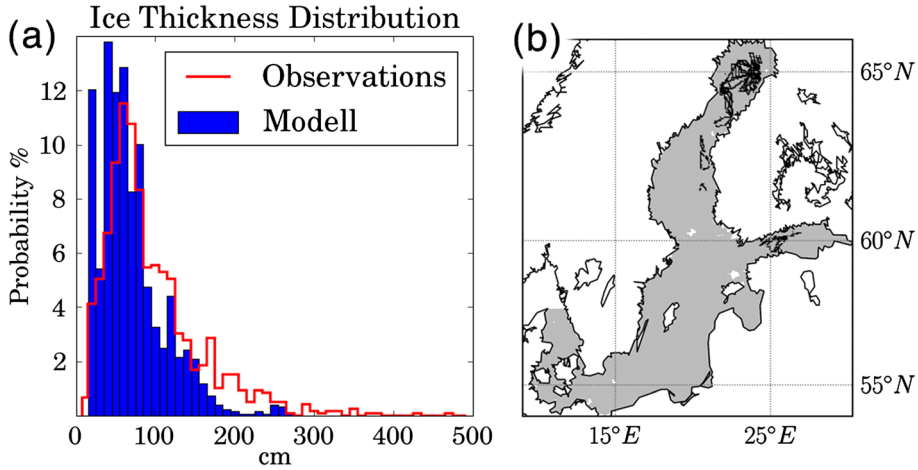

Figure 7. (a) Histograms of ice thickness for gridded EM data (red line) and the corresponding modeled ice thickness (blue). (b) Map of the locations of the EM measurements.

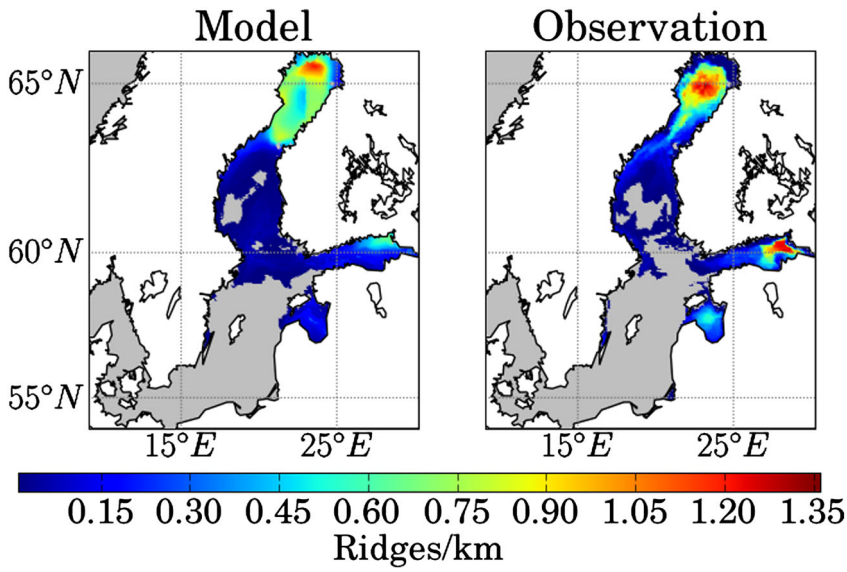

Figure 8. Annual mean simulated ridge density (left panel) and ridge density based on digitized ice charts (IceMap) from the Swedish Ice Service at SMHI (right panel) (winters 2005–2006 and 2006–2007) [ridges/km]. Gray shaded regions correspond to a ridge density below 0.01.

pattern of the standard deviation of ridged ice concentration resembles that of the mean, while gradients toward the center of the sub-basin are weaker. Here, the standard deviations exceed the mean values, reflecting the large interannual variability of the Baltic Sea ice conditions. In contrast, the standard deviation of the ridged ice thickness is largest in regions that are often, but not always, ice covered (Figure 9d). This agrees well with the earlier finding of *Leppäranta* [1981] that the mean thickness of ridges does not vary much. Thus, the interannual variability is dominated by the position of the ice edge (respectively, the line where the ice thickness reaches the threshold thickness between ridging and rafting) rather than by deformed ice properties. Hence, we focus mainly on the analysis of total ridged ice fraction when regarding the interannual variability in the following. Furthermore, no statistically significant trend in the deformed ice properties is found for the period 1962–2007. Linear trends were calculated locally for every model grid point. Strongest trends in the simulated ridged ice fraction occur in the eastern parts of all sub-basins and are in the parts-per-thousand range per decade. Also, the simulated trends in the deformed ice thickness are negligible.

[21] The mean seasonal cycles of deformed and undeformed ice concentrations per ice-covered model grid box are charted in Figure 10 for the two sub-basins with strongest ridging, the Bothnian Bay and the Gulf of Finland. The corresponding basin borders are depicted in Figure 1. The ice concentrations in both sub-basins grow relatively continuously until a maximum is reached, generally in late February or March. During these months, the variability in total ice concentration is largest, compared to ice concentrations earlier and later in the season. In the Bothnian Bay, maximum

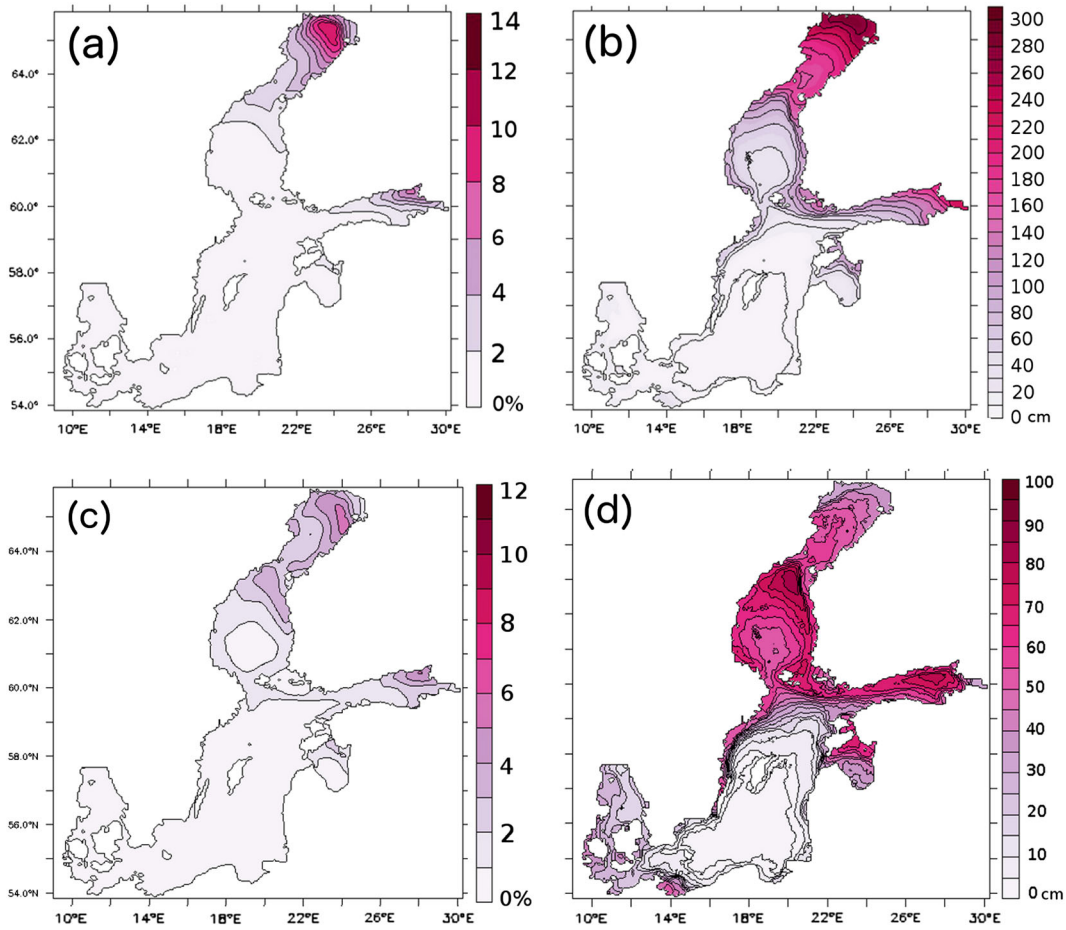

Figure 9. (a) Long-term annual mean (DJFMA, 1962–2007) of simulated ridged ice fraction and (b) ridged ice thickness. Contour levels are 2% for Figure 9a and 20 cm for Figure 9b. (c) Standard deviation of simulated annual mean (DJFMA, 1962–2007) ridged ice fraction and (d) ridged ice thickness. Contour levels are 2% for Figure 9a and 5 cm for Figure 9d. Additional low levels are added at 1% and 1 cm, resp. to illustrate the area of ridging.

ice concentrations are on average 83% and rarely below 50%. In the Gulf of Finland, the mean maximum ice concentration is lower. The mean is 65% but also values of 30–40% are frequent. In severe winters, mean ice concentrations in both sub-basins can reach more than 90%. The seasonal cycles of undeformed, ridged, and rafted ice differ, and the fraction of deformed ice increases throughout the season. Ice deformation usually starts in December or January. Ridged ice concentrations increase throughout the season, while rafted ice concentrations level off in February. Since ridged ice melts away much slower than the thinner level ice, the fraction of deformed ice increases strongly during the melt season. Toward the end of the melt season, rafted ice disappears earlier than ridged ice, and in the end only the once thick ridged ice remains. Accordingly, the variability for ridged and rafted ice is highest toward the end of the ice season. In both subbasins, but more pronounced in the Bothnian Bay, the melting period can be divided into three different phases. The first part of the melting is characterized by the reduction of undeformed ice during March–May. Once the undeformed and rafted ice has melted, the total ice concentration remains constant for a couple of weeks. During that time, the ridged ice continuously becomes thinner until the ice-covered area starts to reduce again. In the Gulf of Finland, this chronology is less pronounced due to less ridged ice.

4.2. Drivers and Proxies of Interannual Ridged Ice Variability

[22] Since the NAO index is a frequently used measure for the mean winter conditions in Northern Europe [*Hurrell*, 1995; *Hurrell and Deser*, 2009], its impact on Baltic Sea ice is of interest. Reflecting the strong coupling to air temperature, a strong correlation between NAO index and Baltic Sea ice extent was demonstrated by several studies [e.g., *Tinz*, 1996; *Jevrejeva and Moore*, 2001; *Jevrejeva et al.*, 2003; *Koslowski and Loewe*, 1994]. In accordance, the mean modeled ice fractions in the Gulf of Finland and Bothnian Bay show a similar variability and are significantly anticorrelated to the NAO index (−0.58, resp. −0.46). Since high ice concentrations are a precondition for ridge formation and the annual mean ridged ice fraction is almost everywhere highly correlated with the mean ice concentration (correlations between 0.65–0.8 in the Bothnian Bay and 0.8–0.9 elsewhere), one would likewise expect a negative

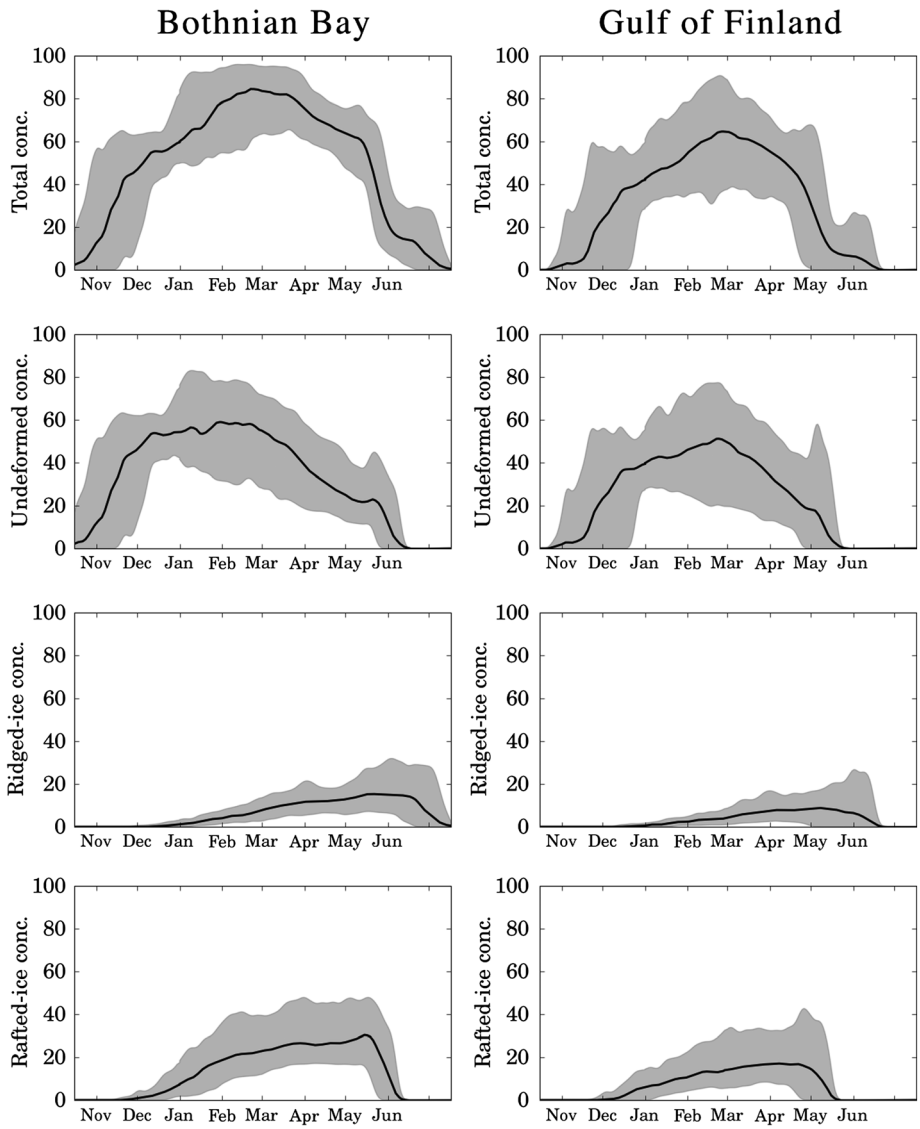

Figure 10. Basin averaged ice concentrations per ice-covered model grid box for the different ice types (from top to bottom, total ice cover, undeformed, ridged, and rafted ice) in the Bothnian Bay and Gulf of Finland (left and right columns, respectively) for the period 1962–2007. The thick line shows the mean seasonal cycle, and the shaded area refers to the 5 and 95 percentiles. The figure is based on a sampling rate of 48 h.

correlation between NAO and ridged ice fraction. However, this relationship is more complex, and the spatial correlation pattern between the NAO index and annual mean deformed ice properties is weakly positive in a large part of the Bothnian Bay, which is (almost) every winter ice covered, and negative otherwise. This reflects the fact that if ice is formed despite relatively mild winter conditions (which happens frequently in the northern part of the basin), the strong winds can promote the formation of ice ridges. Maximum explained variances result from negative correlations. They are obtained in the center of the Gulf of Finland and in the southern Bothnian Bay and amount to a maximum of 25%. Thus, the relationship of ridged ice fraction to the atmospheric forcing conditions is more complex than for ice extent and needs to be considered in more detail: On short time scales (hours–weeks), ice growth is mainly governed by the temperature gradient between ice bottom (SST) and ice surface (air temperature). Additionally, wind influences ice concentrations by distributing the ice. Thus, several atmospheric parameters (e.g., wind, precipitation, air temperature, humidity, radiative fluxes) are involved. On interannual time scales, however, we obtain closely related net radiative fluxes and air temperature in the regularly ice-covered regions. Thus, 2 m air temperature, which is strongly reflected by the NAO index, turns out to be a relatively well-suited proxy for the ice coverage of the Baltic Sea. Since a high ice coverage is a precondition for ice deformation, air temperature indirectly also influences ice deformation and can thus serve as a proxy. However, to use temperature alone as proxy for ice deformation is, as expected, not sufficient, and to obtain satisfactory explained variances, wind has to be used in addition. But as shown above, the consideration of westerlies only, as

summarized in the NAO index, is a too simple approach. The wind advects the ice floes, and with them the ridges and strong wind events lead to the formation of new ridges. The influence of the wind can thus be expected to depend strongly on its direction. Topography also plays an important role, and the wind effect strongly increases near the coast. Also, sea ice motion, which can result in the formation of ridges, depends on the wind stress rather than wind speed. We thus expect the influence of wind to be highly nonlinear and correlate testwise ridged ice fraction against mean wind speed as well as the mean square of the wind speed (closely related to wind stress) and winter mean wind extremes (calculated as described in section 2.4). For mean winds as well as the mean square wind speeds, the absolute values of the correlations are generally below 0.35—apart from limited regions. Higher correlations are obtained when considering the winter mean extreme winds. Taking 2 m air temperature as well as the wind extremes from the four cardinal directions (north, south, east, and west) as a proxy, we perform at each model grid point a multilinear regression on ridged ice fraction to reconstruct the ridged ice area fraction based on these five proxies. Figure 11a shows the pointwise correlations between the reconstruction, obtained by the multilinear regression, and originally simulated ridged ice fraction. Correlations are generally very high in the western part of the Bothnian Bay and Bothnian Sea as well as in the northern part of the Gulf of Finland and Gulf of Riga. All these regions are characterized by comparably cold sea surface temperatures on the upwelling side of the Baltic Sea. By adding modeled SST as a proxy, the rather low correlations (0.45–0.5) in the eastern Bothnian Sea and the southern part of the Gulf of Finland are considerably enhanced (Figure 11b). Now, correlations are significant and sufficiently high everywhere except for the eastern part of the Bothnian Bay. Figure 12 demonstrates that a more detailed quantification of the influencing factors is difficult to obtain since 2 m air temperature is in large areas strongly related to the extreme winds. While for extreme northerly winds, correlations with 2 m air temperature are rather low, southerly and westerly extreme winds are positively correlated with air temperature. For these two components, correlations reach values up to 0.5–0.6 in the northern part of the Baltic and the Gulf of Finland. Also, pronounced easterly extreme winds are related to anomalous cold 2 m air temperatures in a relatively restricted area in the southwestern part of the Baltic Sea. There, the correlations reach values down to −0.7, while the correlations are rather weak in all other parts of the Baltic Sea. This holds especially in the severely ice-covered regions. It is thus most difficult to distinguish the effect of extreme winds on ice deformation from air temperature in the northern Baltic and the Gulf of Finland when regarding the southerly and westerly wind components. However, if ice concentrations are given, the extreme winds in the four cardinal directions provide a very good proxy for ridging, leading to an almost perfect agreement between modeled and reconstructed ridges (Figure 13). We thus determine the major effects of the annual mean extreme winds. In a first step, we investigate the four cardinal wind directions separately by correlating these to ridged ice fractions. The maxima of these four correlations are considered to determine the strength of the main wind effect in a second step. Other wind directions have some noticeable but weaker influence. The corresponding wind directions are merged in a spatial map to illustrate in which region which wind direction has the strongest influence (Figure 14). The associated correlations are overlayed as contour lines. In large parts of the basin, southerly winds have the strongest impact. The corresponding correlations are negative (apart from a small area in the Bothnian Bay). Since southerly winds are strongly related to air temperature (Figure 12), it cannot be quantified statistically whether the temperature effect or displacement of the ice toward the north has a stronger impact. Otherwise, except for some parts of the Bothnian Sea, offshore extreme winds have the dominant impact on ridge formation. Since strong offshore winds lead to the formation of extensive coastal leads (i.e., a significant reduction in the total ice area fraction) and ridging is strongly prevented, the correlations are negative. In particular, the dominance of easterly winds in the very northeast of the Bothnian Bay explains why this region has lower correlations in Figure 11 than any other region. Easterly wind extremes have no correlation with 2 m air temperature (Figure 12), and hence the temperature-dependent multilinear regression model fails in this particular area.

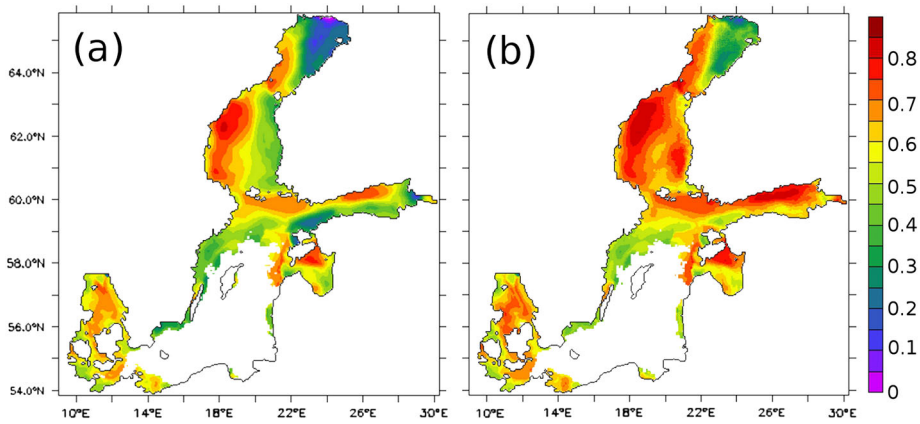

Figure 11. Correlation between reconstructed and originally simulated annual mean ridged ice fraction using a multilinear regression of (a) 2 m air temperature and wind extremes (in north, south, east, and west directions) and (b) same variable as for Figure 11a but including additionally SST as a proxy.

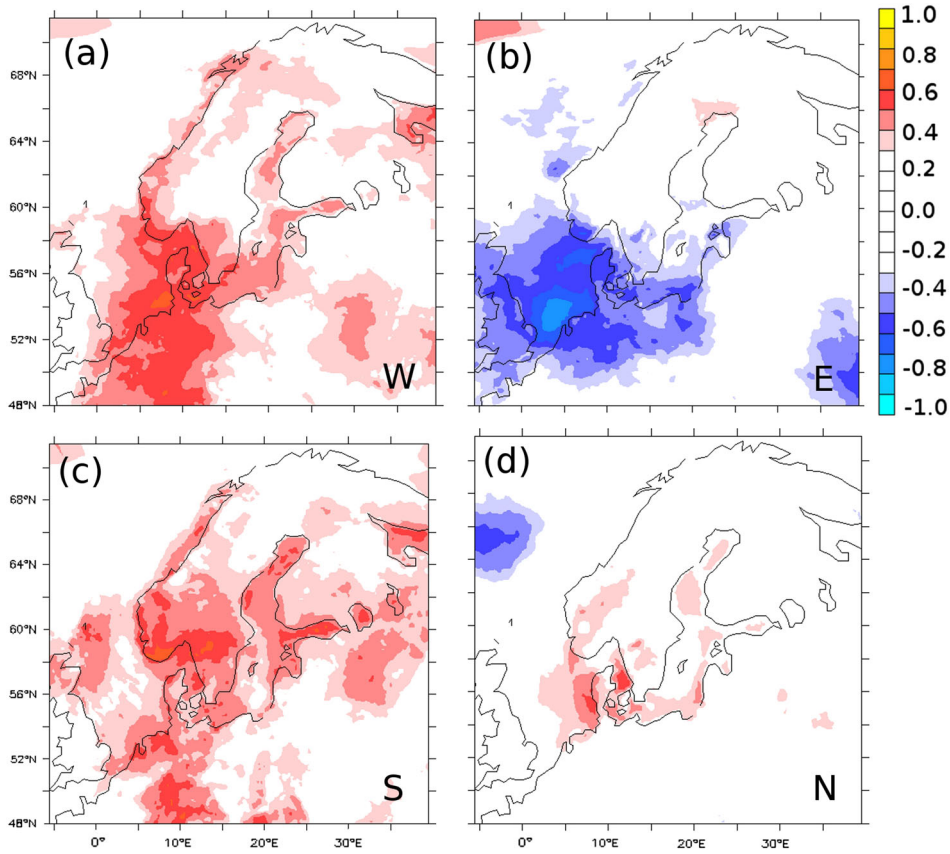

Figure 12. Pointwise linear correlation between winter mean 2 m air temperature and the winter mean monthly wind extremes in (a) west, (b) east, (c) south, and (d) north directions (DJFMA, 1962–2007).

[23] The correlations result in explained variances which are, in the Bothnian Sea, lower than the air temperature-related values, while the pattern is more large scale. In the Bothnian Bay, locally up to 50% of the variance of ridged ice might be explained by the first order (=strongest) wind

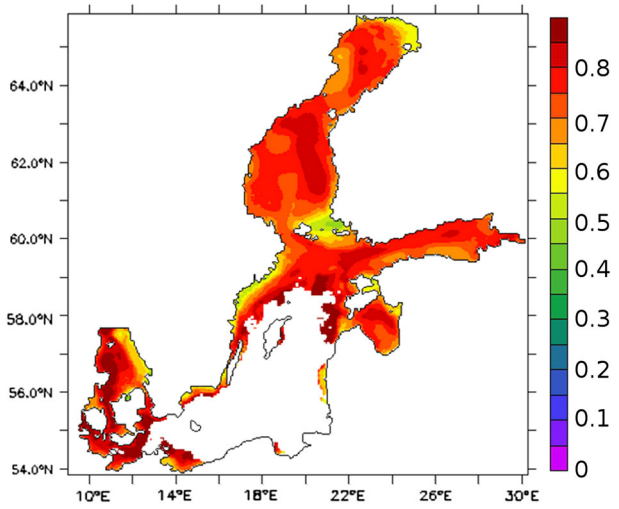

Figure 13. Correlation between reconstructed and originally simulated annual mean ridged ice fraction using a multilinear regression of ice concentrations and wind extremes (in north, south, east, and west directions).

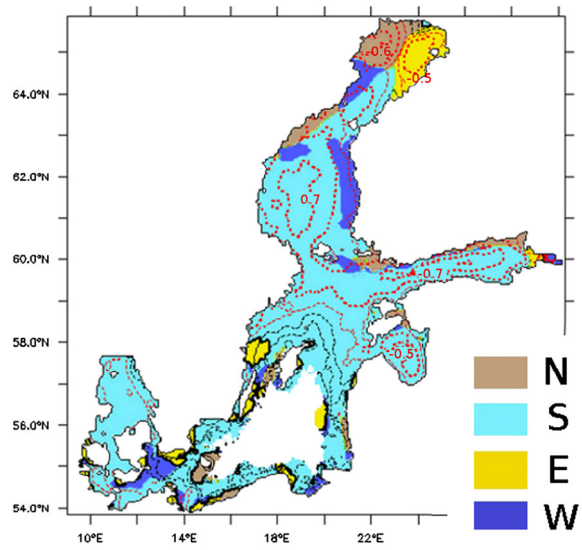

Figure 14. Map of the wind directions corresponding to the maximum wind effect on ridged ice fraction. The contour lines depict the corresponding correlations. Dashed contours denote negative correlations, while solid lines denote positive correlations. Contour levels are 0.1. Contours above 0.5 and below −0.5 are drawn in red.

effect and more than 60% are reached at the eastern coast. In the Gulf of Finland, the major effect is highest in the middle of the sub-basin and amounts to 45% for ridged ice fraction.

[24] Note that the above results hold for ridged ice area fraction and might differ when considering the fraction of deformed ice from the ice present. We thus consider additionally ridge density which is proportional to the latter. Figure 15 shows a linear regression map of the winter mean (DJFMA) monthly maxima of wind speed in the four cardinal directions on simulated ridge density. Also for ridge density, the negative effects of offshore extreme winds by preventing ridging dominate, and the wind-induced increase in ridging is restricted to relatively small regions close to the corresponding coast due to strong onshore winds. Unusual strong easterly winds have the most striking effect. Ice concentrations are lowered on the eastern side of the sea, and the usually strong ridging in this region is prevented. An increase of the winter mean monthly wind extremes of 1 m/s in east direction leads to around 0.5 less ridges/km in the eastern Bothnian Bay, while the amount of ridges in the Gulf of Finland and the eastern Bothnian Sea are reduced by up to 0.18 and 0.3 ridges/km, respectively. Although this negative influence dominates, anomalous strong ridging occurs on the western side of the Bothnian Bay and Bothnian Sea. Especially in the Gulf of Finland, the positive effect can be as strong as the negative effect but is confined to a much smaller region.

5. Discussion

[25] The study successfully determines a link from ridged ice characteristics (spatial and temporal variability) to regularly observed quantities, such as surface air temperature and winds, while an easier link to the NAO index is not satisfactory. But, as stated by *Kauker and Meier* [2003], the NAO is not always a good proxy for the zonal wind component in the Baltic Sea region, and it is thus possible that the latter correlations would increase when considering the Baltic Sea index (BSI) as defined by *Lehmann et al.* [2002] instead of the NAO. However, due to the strong correlation between NAO index and the BSI, we do not expect the results to change drastically. This holds especially since the wind direction relative to the location of the nearest coast turned out to be one major factor, while both indices focus on westerlies. We decided to focus on the NAO index since it is more common. Also, the suggestion of *Chen and Li* [2004], who state that the relation between NAO index and maximum annual sea ice extent changes with time, cannot be confirmed due to the still limited amount of available data. Especially the rather complex multilinear regression

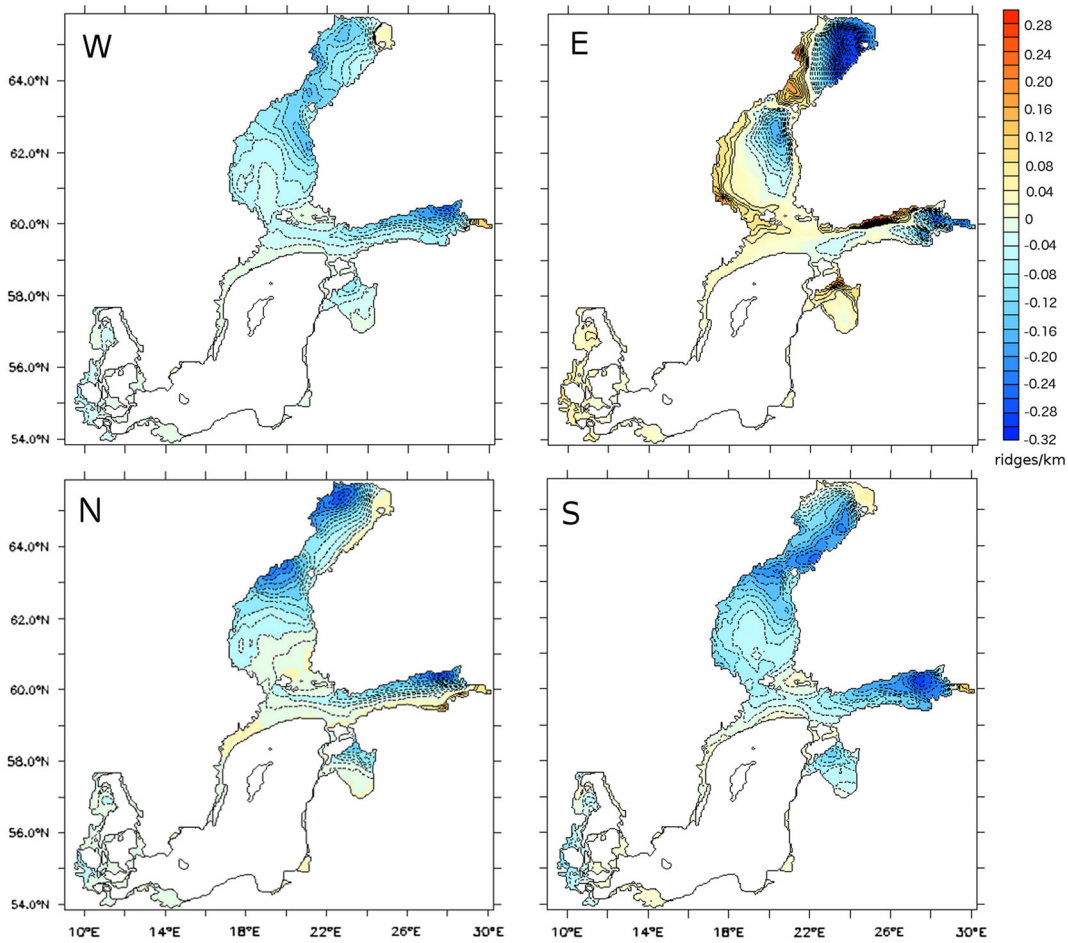

Figure 15. Linear regression of the winter mean (DJFMA) wind extremes in the four basic directions (west, east, north, and south) on ridge density [ridges/km].

could not be performed if not assuming stationarity in time for all relationships. To extend the modeling period would require an extension of the forcing data set, and a detailed analysis of historical data would be needed. Also, it was argued by *Koslowski and Loewe* [1994] that the nonstationarity is related to changes in the NAO pattern rather than to changes in the ice properties. In this case, the results of the multilinear regression would not be affected. Moreover, the results obtained by the regression are in line with the results presented by *Haapala* [2000], who performed a case study of simulated ridges during strong southwesterly winds during winter 1994. Similarly to our results, he states that strong onshore winds lead to an intensive new formation of ridges limited to a relatively narrow zone along the coasts.

[26] However, the results of this study are based on a complex ocean-sea ice model. Such models are still difficult to validate even though we used several available data sources. Also, we identified some model deficiencies, like systematically underestimated ice thickness as well as too low ice concentrations in the Gulf of Riga and the basin interior of the Bothnian Sea. As a direct effect of the too thin ice in the model, one might expect a bias toward rafting compared to ridging since the simulated ice thickness strongly influences the proportion between rafting and ridging. Here it is important to note that the threshold thickness distinguishing rafting from ridging is purely empirical, and a change of this value might influence the results in a similar way. The threshold thickness is an average thickness based on empirical findings and the Parmerter law [*Parmerter*, 1975]. The law states that the maximum thickness for rafting is proportional to the square of the critical ice stress, σ_c. Younger ice is generally weaker than older ice with typical values ranging around $10^6 < \sigma_c < 3.5 \cdot 10^6$ in the Arctic. The Baltic consists of very young ice, which means typical values in the lower range. A threshold thickness of 8 cm was chosen after personal communication with Jari Haapala, FMI (2012). However, possible thresholds span a relatively wide range, which allows for some potential tuning of the ratio of ridged and rafted ice. A wrong proportion between rafted and ridged ice very likely does not influence the correlation patterns strongly, but the amplitude of the regression is likely sensitive to this ratio. Another indirect effect of a deficient ice thickness is the influence on ice mass and with it the ice velocities. The deficiencies in the ice velocities due to systematically too thin ice might be partly compensated by an increased ice strength. Future measurements of ice velocities might lead to further model improvement. However, our results stress that a correct simulation of ice concentrations is crucial, and in particular the ridging in the Gulf of Riga is very likely strongly influenced by the underestimation of ice concentrations in this region. Thus, future model testing and improvement is an ongoing process. Here, indications about where and when to measure are helpful, and a quantification of the impact of the main drivers is an important step forward. While better products of ice concentrations will be available in the near future, due to upcoming satellite products, the precise impact of the winds on ice deformation will still be difficult to determine. It requires more detailed observations which are costly—especially when the area of interest is far from the usual shipping routes. Ridges during March/April contain the integrated effect of the prevailing season. Thresholds for the extreme wind category must be defined specifically for different basins. These can be derived from Figure 2, which depicts the winter wind distributions over (a) the Gulf of Finland, (b) the Bothnian Bay, and (c) the Bothnian Sea. While in the Bothnian Bay easterly winds of 4 Beaufort (Bft) would count as very extreme already, 5 Bft occasionally occur. In contrast, winds of 5 Bft and more are rather frequent in the Bothnian Sea.

6. Summary

[27] The investigation of sea ice deformation in the Baltic Sea is a subject of general interest since it strongly disrupts the intense ship traffic. To predict the formation of sea ice ridges is thus crucial. At the same time, comprehensive long-term observations do not exist. While precise, direct observations are costly and sparse, large-scale patterns are often derived from satellites and contain rather rough estimates. In the present analysis, we investigate the long-term behavior of ridged ice and analyze the main drivers and proxies of ice deformation in a model. Long-term, dynamically downscaled ERA-40 data enable a 40 year hindcast simulation of a new implementation of the coupled ocean-ice model RCO-HELMI for the Baltic Sea. The model was extended from an earlier version to resolve ridged ice and is evaluated as far as possible at present state of available observations. It is demonstrated that the North Atlantic Oscillation (NAO) alone is not a good predictor to explain sea ice deformation in the Baltic Sea since it merges two effects—strength of the westerlies and air temperature, which have here contradictory effects. The explained variances of the ridged ice fraction are below 20–25% in the entire Baltic Sea. In contrast, high local correlations (around 0.8) to ridged ice fraction are obtained, when reconstructing the annual mean ridges by regressing against winter average wind extremes in north, south, east, and west directions, 2 m air temperature, and SST. In large parts of the basin, it is sufficient to use the atmospheric parameters as a predictor, while in the eastern Bothnian Bay and southern Gulf of Finland the long-term memory of the ocean is required. This suggests that the bulk of late winter ridge density can be derived from air temperature, wind, and SST estimates, which are often routinely measured. Once the ice concentrations are given, the winter mean extreme winds in the four cardinal directions provide an almost perfect proxy for annual mean ridged ice fraction. To first order, offshore winds dominate the variability by lowering the ice concentration and thus preventing ridging. Strongest positive effects are obtained close to the coast in combination with strong onshore winds. According to our findings, a focus on observations of ice deformation, drift velocity, and concentration during and after unusual strong onshore as well as offshore winds might be useful.

[28] **Acknowledgments.** This study was performed within the EU-funded project "Safety of winter navigation in dynamic ice" (contract SCP8-GA-2009-233884-SAFEWIN). The RCO-HELMI model simulations were partly performed on the climate computing resources "Vagn" and "Ekman" that are operated by the National Supercomputer Centre (NSC) at Linköping University and the Centre for High Performance Computing (PDC) at the Royal Institute of Technology in Stockholm, respectively. These computing resources are funded by a grant from the Knut and Alice Wallenberg foundation. We are thankful for these supports. Validation data were kindly provided by the "Swedish Ice Service" at SMHI (Swedish Meteorological and Hydrological Institute). We also thank

Karin Borenäs for the supply of drifter data that were collected during the EU-project IRIS (contract EVK3-CT-2002-00083). Christian Haas provided EM-thickness measurements that were collected within the same project. The copyrights for Figure 6b was kindly provided by Tellus A. Jari Haapala kindly provided the HELMI model. Furthermore, we would like to thank Jari Haapala, Lars Axell, and Christian Dieterich, for helpful comments. Last but not least, we would like to thank two extremely helpful anonymous reviewers that would have deserved a coauthorship. Especially one of them was outstanding.

References

Chen, D., and Li, X. (2004), Scale-dependent relationship between maximum ice extent in the Baltic Sea and atmospheric circulation. *Global Planet. Change*, *41*, 275–283.

Haapala, J. (2000), On the modelling of ice-thickness redistribution. *J. Glaceology*, *46*, 427–437.

Haapala, J., N. Lönnroth, and A. Stössel (2005), A numerical study of open water formation in sea ice. *J. Geophys. Res.*, *110*, doi:10.1029/2003JC002200.

Haas, C. (2004), Airborne EM sea-ice thickness profiling over brackish Baltic sea water. *Proceedings of the 17th international IAHR symposium on ice, June 21–25, 2004, St. Petersburg, Russia, All-Russian Research Institute of Hydraulic Engineering (VNIIG), Saint Petersburg, Russia*, 1–17.

Haas, C., J. Lobach, S. Hendricks, L. Rabenstein, and A. Pfaffling (2009), Helicopter-borne measurements of sea ice thickness, using a small and lightweight, digital EM system. *J. Appl. Geophys.*, *67*, 234–241.

Höglund, A., Meier, H. E. M., Broman, B., and Kriezi, E. (2009), Validation and correction of regionalized ERA-40 wind fields over the Baltic Sea using the Rossby Centre Atmosphere model RCA3. 0. *Report Series Swedish Met. and Hydr. Institute (SMHI), Oceanography*, **97**, pp. 35.

Holland, M. M., C. M. Bitz, E. Hunke, W. H. Lipscomb, and J. L. Schramm (2006), Influence of the sea ice thickness distribution on polar climate in CCSM3. *J. Climate*, *19*, 2398–2414.

Hordoir, R. and H. E. Meier, 2010: Freshwater fluxes in the Baltic Sea: A model study. *J. Geophys. Res.*, *115*. doi:10.1029/2009JC005604.

Hunke, E. C., and J. K. Dukowicz (1997), An elastic-viscous-plastic model for sea ice dynamic. *J. Phys. Ocean.*, *27*, 1849–1867.

Hurrell, J. W. (1995), Decadal trends in the North Atlantic Oscillation and relationships to regional temperature and precipitation. *Science*, *269*, 676–679.

Hurrell, J. W., and C. Deser (2009), North Atlantic climate variability: The role of the North Atlantic Oscillation. *J. Mar. Syst*, *78*, 28–41.

Jevrejeva, S. and J. C. Moore (2001), Singular spectrum analysis of Baltic Sea ice conditions and large-scale atmospheric patterns since 1708. *Geophys. Res. Lett.*, *28*, 4503—4506.

Jevrejeva, S., J. C. Moore, and A. Grinsted (2003), Influence of the Arctic Oscillation and El Nino-Southern Oscillation (ENSO) on ice conditions in the Baltic Sea: The wavelet approach. *J. Geophys. Res.*, *108*, doi:10.1029/2003JD003417.

Kankaanpää, P. (1988), Morphology of a Baltic Sea ice pressure ridge. *Geophysica*, *24*, 15–33.

Kankaanpää, P. (1997), Distribution, morphology and structure of sea ice pressure ridges in the Baltic Sea. *Fennia*, *175*(2), 139–240.

Kauker, F., M. Meier (2003), Modeling decadal variability of the Baltic Sea: 1. Reconstructing atmospheric surface data for the period 1902–1998. *J. Geophys. Res.*, *108*, doi:10.1029/2003JC001797.

Koslowski, G., and P. Loewe (1994), The western Baltic Sea ice season in terms of a mass-related severity index: 1879–1992, Part 1. Temporal variability and association with the North Atlantic Oscillation. *Tellus A*, *269*, 66–74.

Lehmann, A., Kraus, W., and Hinrichsen, H. H. (2002), Effects of remote and local atmospheric forcing on circulation and upwelling in the Baltic Sea. *Tellus A*, *54*, 299–316.

Lehmann, A., Getzlaff, K., and Halaß, J. (2011), Detailed assessment of climate variability of the Baltic Sea area for the period 1958–2009. *Clim. Res.*, *46*, 185–196.

Lensu, M. (2003), The evolution of ridged ice fields. *Dissertation Helsinki University of Technology*.

Leppäranta, M. (1981), On the structure and mechanics of pack ice in the Bothnian Bay. *Finnish Marina Research*, *248*, 3–86.

Leppäranta, M., and R. Hakala (1992), The structure and strength of first-year ice ridges in the Baltic sea. *Cold Reg. Sci. Technol.*, *20*, 295–311.

Leppäranta, M., M. Lensu, P. Kosloff, and B. Veitch (1995), The life story of a first-year sea ice ridge. *Cold Reg. Sci. Techn.*, *23*, 279–290.

Leppäranta, M., and K. Myrberg (2009), Physical oceanography of the Baltic Sea. *ISBN* 978-3-540-79702-9, *Springer*, *85*, 296–303.

Löptien, U., and H. E. M. Meier (2011), The influence of increasing water turbidity on the sea surface temperature in the Baltic Sea: A model sensitivity study. *J. Mar. Systems*, *88*, 323–331.

Parmerter, R. R. (1975), A model of simple rafting in sea ice. *J. Geophys. Res.*, *80*, doi:10.1029/JC080i015p01948.

Meier, H. E. M. (2006), Baltic Sea climate in the late twenty-first century: A dynamical downscaling approach using two global models and two emission scenarios. *Clim. Dyn.*, *27*, 39–68.

Meier, H. E. M., R. Döscher, A. C. Coward, J. Nycander, and K. Döös (1999), RCO—Rossby Centre regional Ocean climate model: Model description (version 1.0) and first results from the hindcast period 1992/93. *Reports Oceanography, Swedish Meteorological and Hydrological Institute, SE-60176 Norrkping, Sweden*, **26**, pp. 102.

Meier, H. E. M., R. Döscher, and T. Faxén (2003), A multiprocessor coupled ice-ocean model for the Baltic Sea: Application to salt inflow. *J. Geophys. Res.*, *108*, doi:10.1029/2000JC000.521.

Meier, H. E. M., and F. Kauker, (2003), Modeling decadal variability of the Baltic Sea: 2. Role of freshwater inflow and large-scale atmospheric circulation for salinity. *J. Geophys. Res.*, *108*, doi:10.1029/2003JC001.799.

Monahan, A. H., J. C. Fyve, and G. M. Flato (2000), A regime view of Northern Hemisphere atmospheric variability and change under global warming. *Geophys. Res. Lett.*, *27*, 1139–1142.

Mårtensson, S., M. Meier, J. Haapala, and P. Pemberton (2012), Ridged sea ice characteristics in the Arctic from a coupled multi category sea-ice ocean model. *J. Geophys. Res.*, *117*, doi:10.1029/2010JC006936.

Rogers, J. C. (1997), North Atlantic storm track variability and its association to the North Atlantic Oscillation and climate variability of Northern Europe. *J. Climate*, *10*, 1635–1647.

Saloranta, T. M. (2000), Modeling the evolution of snow, snow ice and ice in the Baltic Sea. *Tellus A*, *52*, doi:10.1034/j.1600-0870.2000.520107.x.

Samuelsson, P., C. G. Jones, U. Willen, A. Ullerstig, S. Gollvik, U. Hansson, C. Jansson, E. Kjellström, G. Nikulin, and K. Wyser (2011), The Rossby Centre regional climate model RCA3: Model description and performance. *Tellus A*, *63*, 4–23.

Seifert, T., and B. Kayser (1995), A high resolution spherical grid topography of the Baltic Sea. *Meereswiss. Ber. 9, Warnemünde, Germany*, 73–88.

Semtner, A. J. (1976), A model for the thermodynamic growth of sea ice in numerical investigations of climate. *J. Phys. Ocean.*, *6*, 379–389.

SMHI and FIMR (1982), Climatological ice atlas for the Baltic Sea, Kattegat, Skagerrak and Lake Vänern (1963–1979). *Distributed by Sjøfartsverket, Norrköping, Sweden*, pp. 220.

Tinz, B. (1996), On the relation between annual maximum extent of ice cover in the Baltic Sea and sea level pressure as well as air temperature field. *Geophysica*, *32*, 319–341.

Timm, O., E. Ruprecht, and S. Kleppek (2004), Scale-dependent reconstruction of the NAO index. *J. Climate*, *17*, 2157–2169.

Uppala, S., et al. (2006), The ERA-40 reanalysis. *Quart. J. Royal Met. Soc.*, *131*, 2961–3012.

Udin, I., S. Uusitalo, J. Sahlberg, A. Seinä, J. E. Lundqvist, and M. Leppäranta (1981), BASIS: A data bank for Baltic sea ice and sea surface temperatures. *Winter Navigation Research Board (Swedish Administration of Shipping and Navigation, Finnish Board of Navigation), Research Report, Norrköping, Sverige*, **34**, pp. 23.

Vihma, T., and J. Haapala (2009), Geophysics of sea ice in the Baltic Sea: A review. *Prog. Ocean.*, *80*, 129–148.

Webb, D. J., A. C. Coward, B. A. de Cuevas, and C. S. Gwilliam (1997), A multiprocessor ocean circulation model using message passing. *J. Atmos. Oceanic Technol*, *14*, 175–183.